ChemPubSoc Europe

DOI: 10.1002/slct.201901737

Chemistry SELECT Full Papers

Organic & Supramolecular Chemistry

Computational Insight Into the Enantioselectivity of Homoboroproline Catalyzed Asymmetric Aldol Reaction

Habibe Dulger,[a, b] Ozlem Sari,[b] Nadir Demirel,[b] and Safiye S. Erdem*[a]

Chiral amino boronic acids and their derivatives have a wide range of applications including enzyme inhibitors, anti-cancer agents and molecular sensors. They also draw attention as effective catalysts. Recently, a new proline based amino boronic acid derivative, homoboroproline, was synthesized and demonstrated to be an efficient catalyst in an asymmetric aldol reaction. The reaction mechanism has been elucidated in the present study for the first time. Considering different orientations of the enamine intermediate and the aldehyde, potential alternative mechanisms were modeled with density functional theory (DFT) calculations via PCM/M06-2X/6-31G(d,p) method in acetone. The potential energy surface of each mechanism was explored to establish the rate-determining and enantioselectivity-determining steps. The calculated enantiomeric excess values (>99%) were found to be in agreement with the experimental values (93%, 95%). The detailed investigation of the transition state structures of the selectivity-determining step has revealed that attractive interactions between boron and aldehyde oxygen are responsible for the selectivity confirmed by natural bond orbital (NBO) analysis. The results provide insight into the origin of enantioselectivity in asymmetric aldol reaction catalyzed by homoboroproline.

Introduction

The aldol reaction, discovered by Wurtz[1] in 1872, serves as powerful method for the construction of C–C bond.[2–5] In particular, asymmetric aldol reactions represent a significant challenge for organic chemists.[6] A number of strategies have been performed to introduce chirality into a molecule such as the use of organometallic or purely organic catalysts.[7] Bifunctional catalysts are probably the most frequently used organocatalysts for numerous applications in synthetic chemistry.[8,9] The most well-known and effective bifunctional catalysts are proline based bifunctional catalysts for both intramolecular and intermolecular aldol reactions.[10–18] Computational investigations of these reactions are well documented.[19–25] In this regard, Houk, List and co-workers developed Houk-List model to elucidate the origin of the enantioselectivity for the proline catalyzed intermolecular aldol reactions.[22,25] The proposed mechanism for the reaction between benzaldehyde (and isopropionaldehyde) and cyclohexanone proceeds through an enamine intermediate (Scheme 1).[22,24,25]

All reasonable potential modes of addition were evaluated (i) the *syn*- and *anti*- orientations of the enamine double bond relative to the carboxylic acid group (ii) two prochiral faces of aldehyde (*re* and *si*) (iii) three staggered arrangements of the aldehyde and enamine around the developing C–C bond (iv) and two half-chair conformations of cyclohexene of the enamine.[22,24,25] All potential products are depicted in Scheme 1.

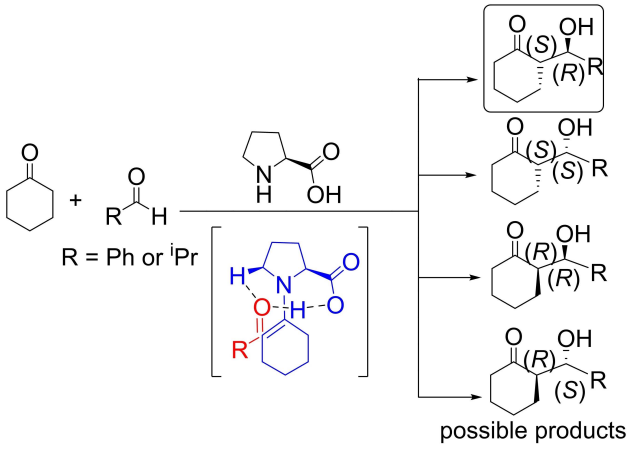

Scheme 1. Potential products for the asymmetric intermolecular aldol reaction[22,24,25]

The most stable transition state involves the *re*-face attack of the *anti*-enamine which leads to the formation of major (*S*,*R*)-isomer (Scheme 1). One of the key interactions contributing to the transition state stabilization is hydrogen bonding interaction between carboxylate and aldehyde. In addition, another electronic stabilization results from NCH•••O interaction as shown in Scheme 1.[22,24,25]

Among the great variety of bifunctional catalysts available in the literature, aminoboronic acids, which possess both Lewis acidic boronic acid and basic or nucleophilic amino groups, look promising as green, metal free catalysts in aldol reactions.[26] The pioneering use of aminoboronic acids was

[a] *H. Dulger, Prof. S. S. Erdem*
Department of Chemistry, Faculty of Arts and Sciences, Marmara University, Goztepe Campus, 34722, Istanbul, Turkey
E-mail: erdem@marmara.edu.tr
[b] *H. Dulger, Dr. O. Sari, Prof. N. Demirel*
Department of Chemistry, Kirsehir Ahi Evran University, 40100, Kirsehir, Turkey

Supporting information for this article is available on the WWW under https://doi.org/10.1002/slct.201901737

reported by Letsinger.[27–30] Over the last 20 years, several direct amide formation and aldol reactions have been described involving aminoboronic acids as catalysts.[31–39]

Recently, Georgiou *et al.*[8] reported an intermolecular asymmetric aldol reaction between *p*-nitrobenzaldehyde and acetone catalyzed by hydrobenzoin boronate ester derivative. The reaction afforded adduct (*S*)-**3** in a good yield and an excellent enantioselectivity (Scheme 2).

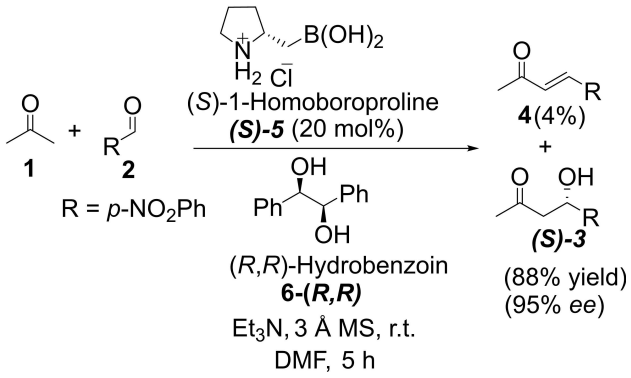

Scheme 2. Intermolecular aldol reaction of p-nitrobenzaldehyde and acetone.[8]

The mechanism proposed by Georgiou *et al.*[8] involves the reaction of homoboroproline (*S*)-**5** with hydrobenzoin **6** which results *in situ* formation of the intermediate (*S*)-1-hydrobenzoin boronate ester (*S*)-**7** (Scheme 3). In the following step, boronate

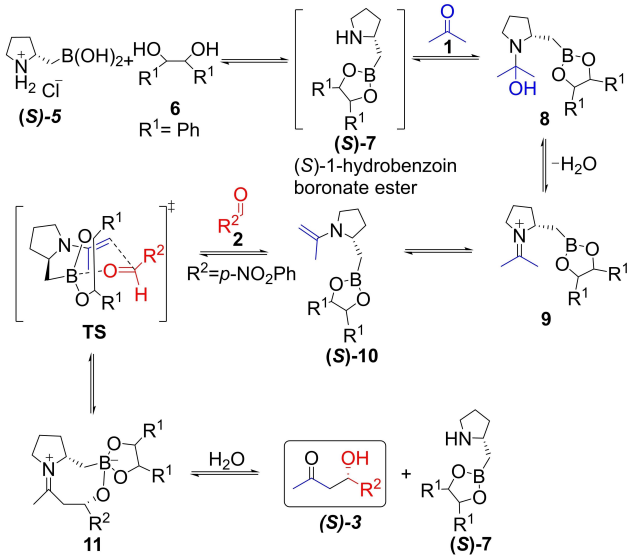

Scheme 3. Proposed mechanism by Georgiou *et al.*[8]

ester (*S*)-**7** could further react with the acetone to furnish amino-alcohol **8**, which then undergoes a dehydration reaction to form iminium ion species **9**. Deprotonation of **9** leads to the formation of enamine (*S*)-**10**. Lewis acid activation of the carbonyl group of the aldehyde **2** with the boronate ester, enables it to react with the enamine (*S*)-**10** via an eight-membered ring transition state **TS**. Finally, hydrolysis of the iminium intermediate **11** affords the aldol product (*S*)-**3** and regeneration of boronate ester (*S*)-**7**. Additionally, by means of dehydration by-product **4** is observed as well (Scheme 3).

The first four steps of the mechanism given in Scheme 3 are very well-known reactions from the previous studies of various similar reactions. The most crucial step is the addition of aldehyde **2** to enamine (*S*)-**10** which is expected to be the enantioselectivity-determining step.

Herein, we investigate the reaction mechanism of intermolecular aldol reaction through understanding of bifunctional role of the hydrobenzoin boronate ester by DFT calculations. The results provide mechanistic insights into the factors that control the stereochemical course of the boronate ester catalyzed aldol reactions.

Results and Discussion

Conformational analysis

Georgiou *et al.*[8] reported that the major factor which contributes to the stereochemistry of the aldol adduct is the stereochemistry of the chiral center of the catalyst. On the other hand, in order to account for the conformational effects, conformational search for the (*S*)-1-hydrobenzoin boronate ester-enamine (*S*)-**10** is necessary before modeling the reaction mechanism. Therefore, conformational analysis for the (*S*)-**10** has been carried out with the molecular mechanics method using force field MMFF (Merck Molecular Force Field) implemented in Spartan14 software. Among several conformers, three stable conformers have been selected which enabled the construction of the proposed transition states. These conformers have been subjected to geometry optimization using the polarizable continuum model (PCM) with M06-2X/6-31G (d,p) method in acetone. Optimized geometries and computed relative energies of (*S*)-**10a**$_{down}$, (*S*)-**10b**$_{up}$ and (*S*)-**10c**$_{up}$ conformers are provided in Figure 1. According to the observed geometries, the orientation of enamine double bond could be syn (down) or anti (up) with respect to the boronate ester group. The computed energies of the most stable up and down conformations indicates that (*S*)-**10a**$_{down}$ has slightly (1.0-1.70 kcal/mol) lower energy than those of (*S*)-**10b**$_{up}$ and (*S*)-**10c**$_{up}$. Since the energy differences between the conformers are small, both orientations of the double bond (up/down) of the enamine have been considered in modeling the mechanism.

To understand the experimentally observed product, we have considered all possible factors that could affect the stereoselectivity; (i) the position of the enamine double bond (up/down) (ii) si/re faces of *p*-nitrobenzaldehyde (iii) two absolute configurations of homoboroproline (*R* and *S*) and (iv) two possible enantiomers of diol (*R*,*R*-hydrobenzoin; *S*,*S*-hydrobenzoin).

Figure 1. Optimized structure of the most stable conformers of the (*S*)-1-hydrobenzoin boronate ester-enamine (***S*)-10**. Relative Gibbs free energies are indicated in kcal/mol. Only selected hydrogen atoms are shown for clarity.[1]

Therefore, ten possible mechanisms have been investigated. The first four mechanisms (**M1**-**M4**) simulate the competing pathways of the reaction with (*S*)-homoboroproline and are discussed below. The next four mechanisms (**M5**-**M8**) represent the pathways of (*R*)-homoboroproline catalyst which are analogous to **M1**-**M4** and have therefore been discussed in Supporting Information. Last two mechanisms (**M9, M10**) have been modeled in order to explore the effect of the diol configuration. In line with the experimental study, the mechanisms occurring through the diol *S,S*-hydrobenzoin have given rise to larger activation energies (See the Supporting Information Figures S12-S15) than their corresponding (*R,R*) diols. Therefore, herein we report the mechanisms occurring through *R,R*-hydrobenzoin which is the diol used in the experimental work.

Mechanism 1 (M1): [(*S*)-homoboroproline (enamine double bond (*down*)) + (*R,R*)-hydrobenzoin + acetone + *p*-NO_2 benzaldehyde → (*S*)-alcohol (*si*-face attack)]

In the experimental study, the reaction of (*S*)-homoboroproline with (*R,R*)-hydrobenzoin results in the formation of *RR*-(*S*)-1-hydrobenzoin boronate ester **7-*RR*-(*S*)** which then reacts with aldehyde **2** to form (*S*)-aldol product selectively. In the computational study, firstly, the attack of enamine to the *si* face of the aldehyde has been considered. Such an approach leads to the formation of the major (*S*)-adduct, which is consistent with the experimental selectivity. Based on our modeling studies, the slightly revised mechanism that we have proposed is outlined in Scheme 4.

We have first located the transition state **M1-TS1**$_{down\text{-}si}$ for the C – C bond formation step of the aldol reaction. As can be seen from Figure 2, the distance between boron and the

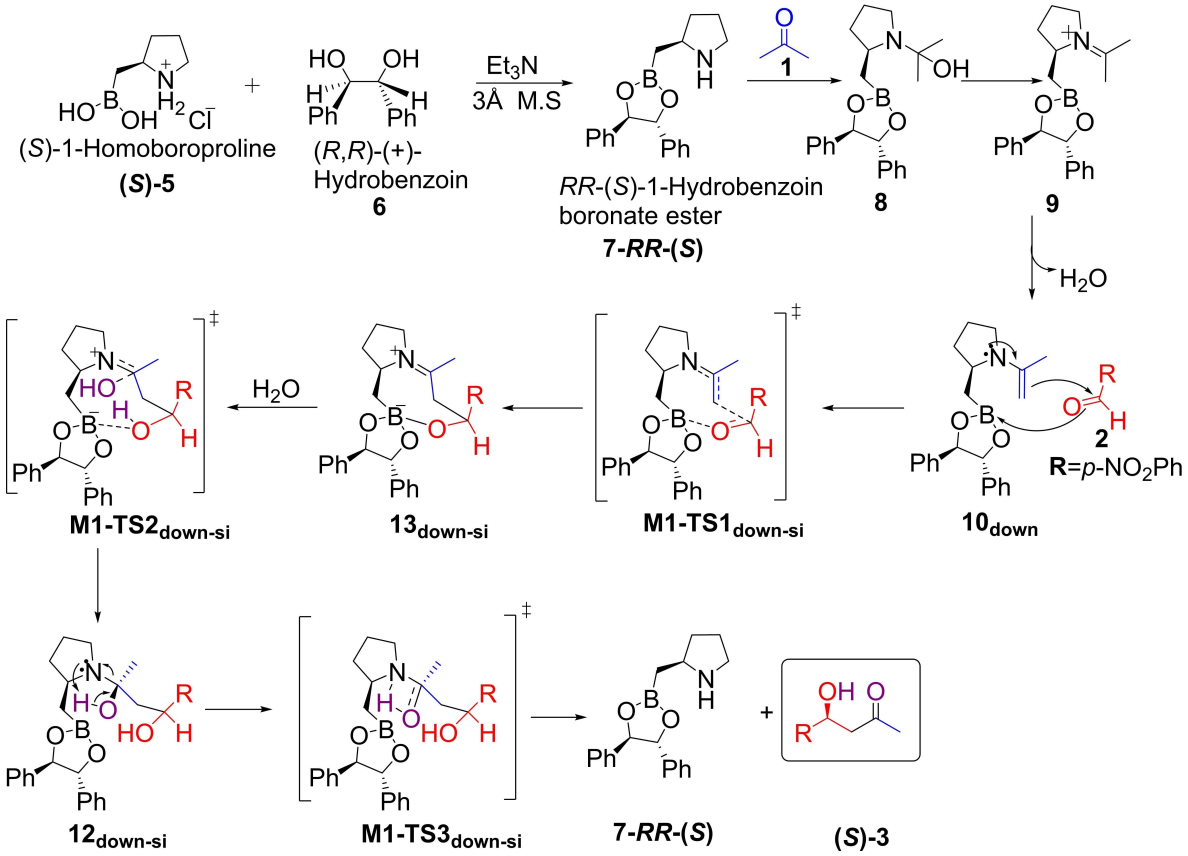

Scheme 4. Our proposed mechanism for the intermolecular aldol reaction catalyzed by homoboroproline

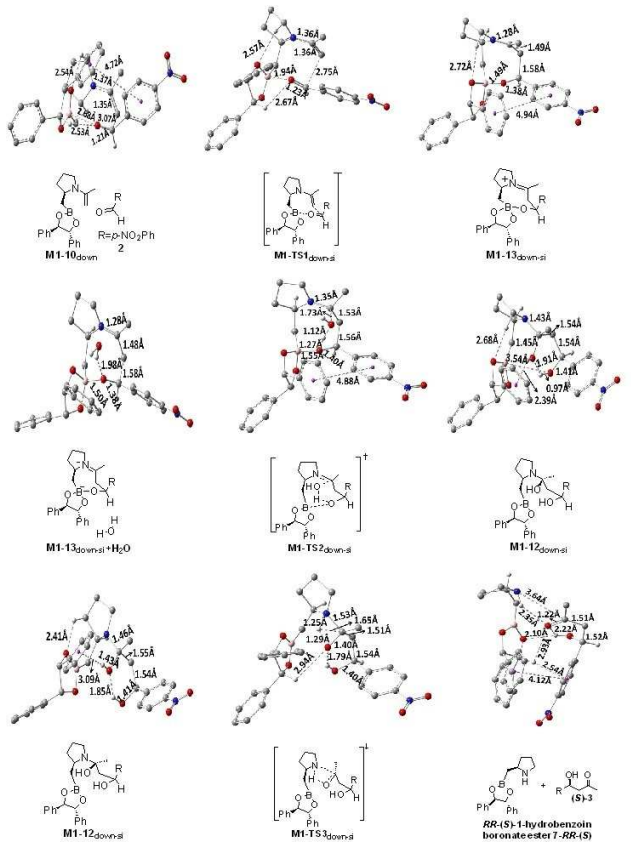

Figure 2. Optimized geometries for stationary points of **M1** at PCM(acetone)/M06-2X/6-31G(d,p) level. Only selected hydrogens are shown for clarity. Distances are given in Å (carbon, gray; hydrogen, white; oxygen, red; nitrogen, blue; boron, light pink)

oxygen atom of carbonyl group is 1.94 Å in the **M1-TS1**$_{down\text{-}si}$. In this step, the C3-C4 bond length shortens from 3.07 Å in **M1-10**$_{down}$ to 2.75 Å in **M1-TS1**$_{down\text{-}si}$. This step can be considered as almost barrierless since it only requires a Gibbs free activation energy of 0.8 kcal/mol and is exergonic by 15.9 kcal/mol (Figure 3).

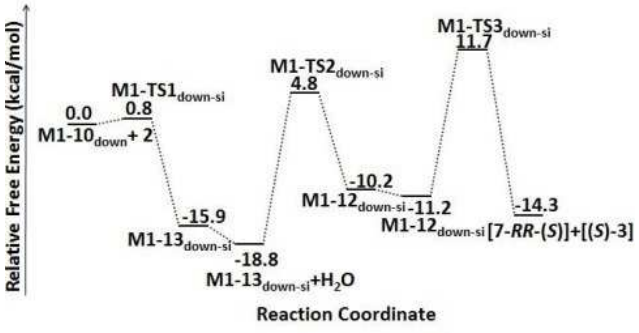

Figure 3. Potential energy profile for **M1** at PCM(acetone)/M06-2X/6-31G(d,p) level. (Relative energies shown for **M1-10**$_{down}$ + **2**, **M1-TS1**$_{down\text{-}si}$ and **M1-13**$_{down\text{-}si}$ include Gibbs free energy of water.)

The second step of this pathway is addition of water which is present in the reaction medium (from the reaction of (*S*)-1-homoboroproline and diol **6** or the enamine formation step). This step takes place through transition state **M1-TS2**$_{down\text{-}si}$ and has a Gibbs free activation energy of 4.8 kcal/mol with respect to the initial reactant complex **M1-10**$_{down}$ + **2**.

In the final step, a proton is transferred from the hydroxyl group (O8H9) to proline nitrogen which is followed by the generation of (*S*)-adduct and the recovery of catalyst. Proton transfer occurs via relatively strain four-membered ring transition state **M1-TS3**$_{down\text{-}si}$. Gibbs free activation barrier is predicted to be 11.7 kcal/mol with respect to the reactant complex **M1-10**$_{down}$ + **2**. Thus, proton transfer step can be considered as the rate-limiting step while C–C bond formation step is the selectivity-determining step.

Mechanism 2 (M2): [(*S*)-homoboroproline (enamine double bond (*down*)) + (*R*,*R*)-hydrobenzoin + acetone + *p*-NO_2 benzaldehyde → (*R*)-alcohol (*re*-face attack)]

The formation of the alternative (*R*)-product can be achieved by the nucleophilic attack of enamine (down) to the *re* face of the aldehyde. Since this is not the preferred face of the attack, only the optimized geometries of the transition states are depicted in Figure 4 (for all stationary points, see the Supporting Information) and energy profile of the reaction is given in Figure 5.

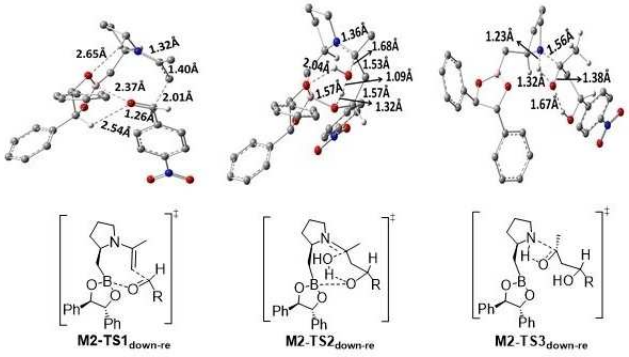

Figure 4. Optimized geometries for transition structures of **M2** at PCM (acetone)/M06-2X/6-31G(d,p) level. Only selected hydrogens are shown for clarity. Distances are given in Å (carbon, gray; hydrogen, white; oxygen, red; nitrogen, blue; boron, light pink)

Among three TSs, the proton transfer step **M2-TS3**$_{down\text{-}re}$ is the highest energy TS. This step, leading to (*R*)-aldol product, requires a Gibbs free activation energy of 19.0 kcal/mol (with respect to **M2-10**$_{down}$ + **2**), which can be overcome at room temperature. However, mechanism **M1** affording the experimentally observed (*S*)-product requires much lower energy than that of **M2**. The relatively high barrier of the proton transfer step indicates that **M2** is less plausible mechanism for the reaction in consideration.

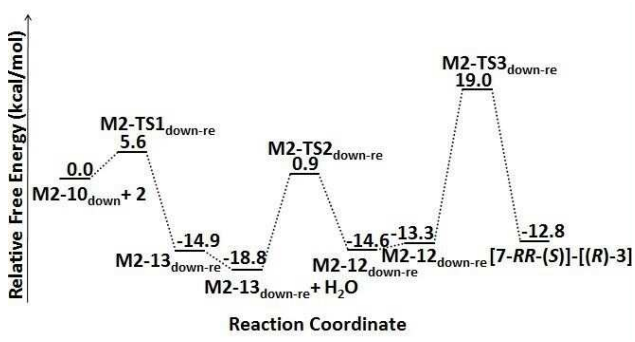

Figure 5. Potential energy profile for **M2** at PCM(acetone)/M06-2X/6-31G(d,p) level. (Relative energies shown for **M2-10**$_{down}$ + **2**, **M2-TS1**$_{down-re}$ and **M2-13**$_{down-re}$ include Gibbs free energy of water.)

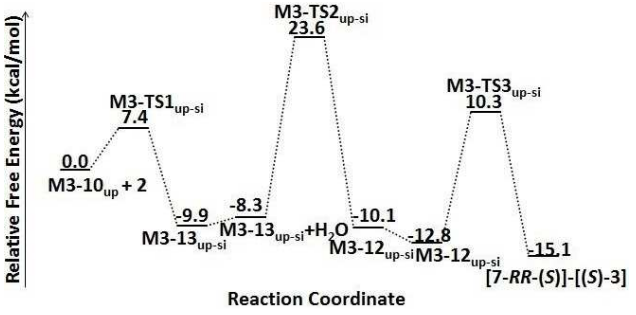

Figure 7. Potential energy profile for **M3** at PCM(acetone)/M06-2X/6-31G(d,p) level. (Relative energies shown for **M3-10**$_{up}$ + **2**, **M3-TS1**$_{up-si}$ and **M3-13**$_{up-si}$ include Gibbs free energy of water.)

Mechanism 3 (M3): [(*S*)-homoboroproline (enamine double bond (*up*)) + (*R*,*R*)-hydrobenzoin + acetone + *p*-NO_2 benzaldehyde → (*S*)-alcohol (*si*-face attack)]

The first step of the **M3** involves the attack of enamine (up) to the *si* face of the aldehyde. The C–C bond formation between the nucleophilic center of the enamine and the carbonyl carbon of aldehyde takes place via eight-membered ring transition state **M3-TS1**$_{up-si}$, which has an higher energy barrier (7.4 kcal/mol) than that of the **M1** (0.8 kcal/mol). Optimized transition structures are given in Figure 6 and the potential energy profile is depicted in Figure 7 (for all stationary points, see the Supporting Information).

The addition of water to zwitter ionic intermediate **M3-13**$_{up-si}$ occurs with an energy barrier of 23.6 kcal/mol with respect to the initial reactant complex **M3-10**$_{up}$ + **2** (Figure 7). Although proton transfer occurs via relatively strained four-membered ring transition state, Gibbs free activation barrier is predicted to be 10.3 kcal/mol with respect to the initial reactant complex **M3-10**$_{up}$ + **2**, which is much lower than that of the second step of **M3**.

Mechanism 4 (M4): [(*S*)-homoboroproline (enamine double bond (*up*)) + (*R*,*R*)-hydrobenzoin + acetone + *p*-NO_2 benzaldehyde → (*R*)-aldol (*re*-face attack)]

This mechanism involves the addition of enamine (up) to the *re*-face of the aldehyde leading to the formation of minor (*R*)-product, which is not consistent with the experimental observation. Modeling this mechanism allows us to verify the experimental result. As can be seen from Figure 8, the C–C bond formation step occurs via 8-membered ring transition state **M4-TS1**$_{up-re}$ with a low energy barrier (for all stationary points, see the Supporting Information).

The second step proceeds through transition state **M4-TS2**$_{up-re}$ and has a Gibbs free activation energy of 12.6 kcal/mol with respect to the initial reactant complex **M4-10**$_{up}$ + **2** (Figure 9).

Proton transfer from hydroxyl group (-O3H4) to proline nitrogen takes place via **M4-TS3**$_{up-re}$ forming the minor (*R*)-

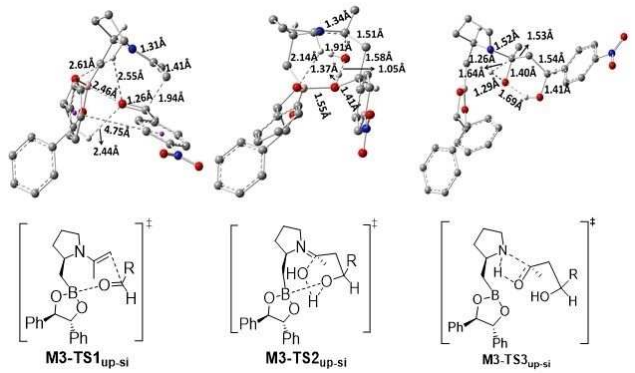

Figure 6. Optimized geometries for transition structures of **M3** at PCM (acetone)/M06-2X/6-31G(d,p) level. Only selected hydrogens are shown for clarity. Distances are given in Å (carbon, gray; hydrogen, white; oxygen, red; nitrogen, blue; boron, light pink)

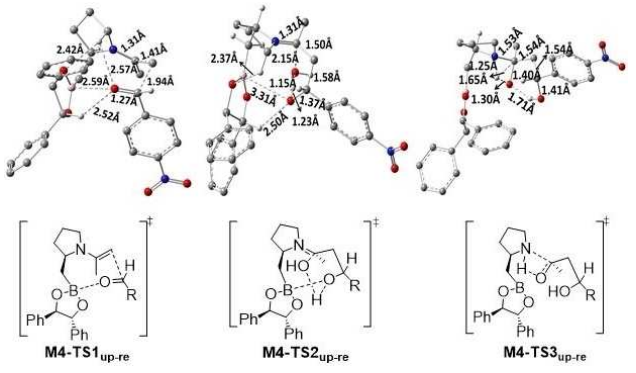

Figure 8. Optimized geometries for transition structures of **M4** at PCM (acetone)/M06-2X/6-31G(d,p) level. Only selected hydrogens are shown for clarity. Distances are given in Å (carbon, gray; hydrogen, white; oxygen, red; nitrogen, blue; boron, light pink)

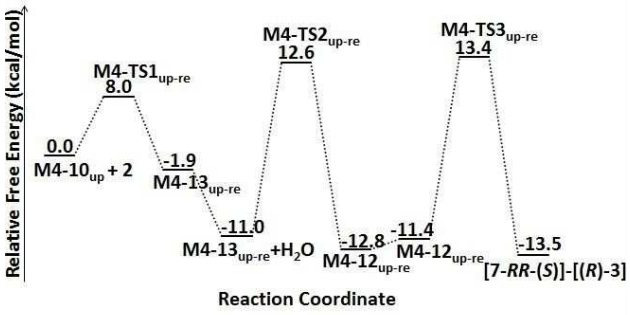

Figure 9. Potential energy profile for **M4** at PCM(acetone)/M06-2X/6-31G(d,p) level. (Relative energies shown for **M4-10$_{up}$ + 2**, **M4-TS1$_{up\text{-}re}$** and **M4-13$_{up\text{-}re}$** include Gibbs free energy of water.)

product which exhibits similar Gibbs free activation barrier as the former step (Figure 9).

Georgiou *et al.*[40] also reported the intermolecular aldol reaction between *p*-nitrobenzaldehyde and acetone catalyzed by (*R*)-homoboroproline. They proposed that the stereochemistry of the product was controlled by the neighboring chiral center of the pyrrolidine ring instead of the chirality of the diol used for the esterification of the boronic acid.[8,26,40] In the case of (*R*)-catalyst, (*R*)-alcohol product was obtained (93% *ee,* 89% yield) as expected.[40] In order to obtain further verification on the reaction mechanism and selectivity, possible pathways of the aldol reaction in the presence of (*R*)-homoboroproline have been also investigated theoretically in the mechanisms **M5** to **M8**. Similar results as in mechanisms **M1**-**M4** have been observed. (For the optimized structures, potential energy profiles and discussion of **M5** to **M8**, see the Supporting Information).

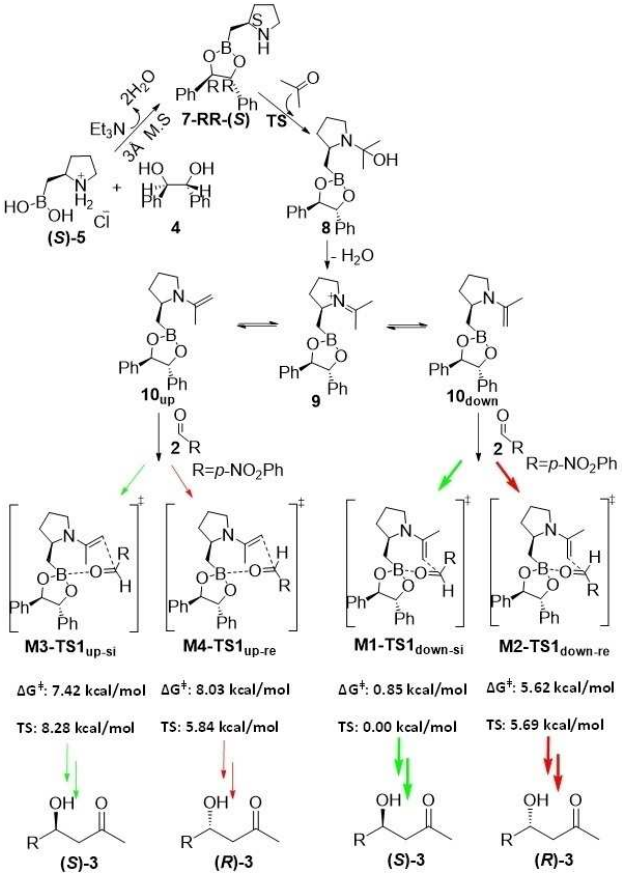

Figure 10. Possible pathways leading to (*R*)- or (*S*)-alcohol products using (*S*)-catalyst and the relative Gibbs free energies of the enantio-determining transition states. Paths leading to the experimentally observed product (***S***)-**3** were depicted by green arrows while the paths producing (***R***)-**3** were colored by red. For the pathways leading to the same alcohol product, preferred one was shown by bold arrows.

Origins of enantioselectivity

Energy profiles of all studied mechanisms reveal that the C–C bond formation occurs readily in the first steps. Therefore, we focus our attention on the first step since it is the enantio-determining step; and explore the key interactions influencing the stabilities of the competing transition states.

We compare four possible pathways for the reaction of aldehyde **2** and acetone in the presence of hydrobenzoin boronate ester **7-*RR*-(*S*)** as the catalyst (Figure 10). Since stereochemistry of the homoboroproline controls the stereochemistry of the reaction, (*S*)-aldol product is expected to be the major product of the reaction. Two alternative paths (down or up orientation of enamine) may lead to the formation of the expected (*S*)-product via mechanisms **M1** and **M3** (Green paths in Figure 10). The relative energies of the corresponding transition states ($\Delta\Delta G^{\ddagger}$) indicate 8.28 kcal/mol preference for the **M1-TS1$_{down\text{-}si}$** over the **M3-TS1$_{up\text{-}si}$**. Besides, the activation barrier for the C–C bond formation step of **M1** is 6.57 kcal/mol lower than that of **M3** (Figure 10). Thus, **M1** is the preferred path leading to the (*S*)-product (highlighted with bold green arrow in Figure 10).

The other two mechanisms (**M2** and **M4**; red paths in Figure 10) lead to the formation of the minor (*R*)-aldol product. The activation barrier for the C–C bond formation step of **M2** is 2.4 kcal/mol lower than that of **M4** (Figure 10). Therefore, the reaction prefers to follow **M2** to furnish the minor (*R*)-product (highlighted with bold red arrow).

Then, we compare each of the most favorable path leading to the (*S*)- and (*R*)-products (**M1** and **M2**, respectively). Overall, **M1** is found as energetically the most favorable mechanism, which leads to the experimentally observed product. The calculated enantioselectivity (>99%) is in favor of the *S*-enantiomer which compares well with the experimental value of 95%.

A similar analysis has been performed for the reaction catalyzed by the (*R*)-catalyst **7-*RR*-(*R*)** in mechanisms **M5**-**M8**. (see Supporting Information Figure S17). The difference in the $\Delta G^{\ddagger}$ values of the most favorable *re* and *si* transition states (**M5-TS1$_{down\text{-}re}$** and **M8-TS1$_{up\text{-}si}$**) is calculated to be $\Delta\Delta G^{\ddagger}_{re/si} =$ 4.64 kcal/mol. The calculated enantioselectivity is >99%, which is in reasonable agreement with the experimental value (93% ee).

In order to provide insight into the origin of enantioselectivity, the geometric features of the crucial transition states have been carefully examined. The enantio-determining **TSs** are shown in Figure 11.

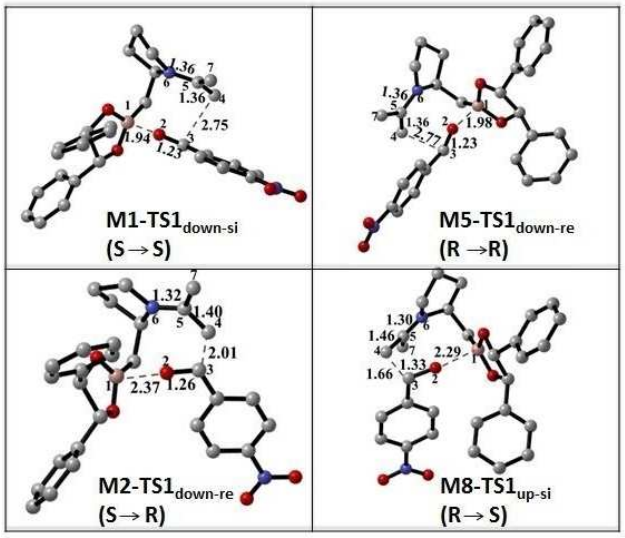

Figure 11. Comparison of the transition states for the C – C bond formation step of homoboroproline catalyzed aldol reaction. Hydrogen atoms are omitted for clarity.

There are two main factors influencing the enantioselectivity of the asymmetric aldol reaction with homoboroproline; (i) the distance between the boron atom (B1) of the catalyst and oxygen atom (O2) of the aldehyde and (ii) the distance between carbon atom (C4) of the enamine and carbon atom (C3) of the aldehyde.

In the lower energy transition states, **M1-TS1**$_{down\text{-}si}$ and **M5-TS1**$_{down\text{-}re}$, the striking feature is the shorter B1-O2 distances revealing the stronger interactions between boron and oxygen. An important question merits attention: What is the main factor that leads to shortening of B1-O2 distance? As can be seen from Figure 11, the B1-O2 distance diminishes with a corresponding increase in the C3-C4 distance. In the most stable TSs, **M1-TS1**$_{down\text{-}si}$ and **M5-TS1**$_{down\text{-}re}$, the C3-C4 distances are calculated as 2.75 and 2.77 Å, respectively. However, in the less stable transition states, **M2-TS1**$_{down\text{-}re}$ and **M8-TS1**$_{up\text{-}si}$, the C3-C4 distances are calculated as 2.01 and 1.66 Å, respectively. The relatively longer C3-C4 distances in **M1-TS1**$_{down\text{-}si}$ and **M5-TS1**$_{down\text{-}re}$ can be attributed to the steric hindrance between methyl group of the enamine and the phenyl group of the aldehyde because both groups occupy the upper part of the forming C3-C4 bond. Such unfavorable interactions do not exist in the case of **M2-TS1**$_{down\text{-}re}$ and **M8-TS1**$_{up\text{-}si}$ since methyl of the enamine is positioned away from the phenyl group of the aldehyde, which leads to a relatively shorter distance between C3 and C4. Presumably, this close proximity of C3 and C4 would increase the B1-O2 distance and weaken the favorable boron-oxygen interaction. The analogous structural differences reported by Sakata and Fujimoto[41] in the reaction of allylboronate with benzaldehyde are in line with our results. Another study by Lai *et al.*[42] on α-amidoboronic acids provides both experimental and computational evidence that the formation of dative-bond between carbonyl oxygen and boron plays a catalytic role in enhancing the rate of amide hydrolysis, which also supports our hypothesis.

In order to provide further insight into stereo-induction, we have investigated the natural bond orbital (NBO)[43] charges. The calculated NBO charges of aldehyde oxygen O2 and boron B1 for **M1-TS1**$_{down\text{-}si}$, **M2-TS1**$_{down\text{-}re}$, **M5-TS1**$_{down\text{-}re}$ and **M8-TS1**$_{up\text{-}si}$ are O2:-0.557 B1: 1.210, O2:-0.746 B1:1.247, O2:-0.550 B1:1.214, O2:-0.878 B1:1.245, respectively which confirm the expected charge transfer interaction. The second order perturbation theory analysis of the Fock matrix in the NBO is a powerful tool to analyze the donor-acceptor interactions in competing transition state structures.[44,45] Therefore, we have analyzed the NBO output and quantified all key B1–O2 interactions between the catalyst and the substrate via stabilization energies (Table 1) for the main competing transition state structures. As observed in Table 1, donor-acceptor stabilization energies mainly stem from the interactions between the lone pair (LP) donor NBO's of O2 and the LP* acceptor NBO's of B1, verifying

Table 1. Donor-acceptor stabilization energies[a] (*E*(2)) obtained from second order perturbation theory analysis of the Fock matrix in NBO.

Donor NBO (*i*)	Acceptor NBO (*j*)	*E*(2) kcal/mol
M1-TS1$_{down\text{-}si}$		
33. BD C3–O2	122. LP* B1	6.70
129. LP O2	120. LP* B1	7.44
129. LP O2	122. LP* B1	11.67
130. LP O2	120. LP* B1	43.83
130. LP O2	121. LP* B1	6.59
130. LP O2	122. LP* B1	51.91
		Total: 128.14
M2-TS1$_{down\text{-}re}$		
128. LP* C3	646. BD* C5–C4	50.17
129. LP O2	121. LP* B1	14.30
130. LP O2	121. LP* B1	8.99
131. LP O2	121. LP* B1	6.73
		Total: 80.19
M5-TS1$_{down\text{-}re}$		
61 BD C3–O2	122. LP* B1	6.68
129. LP O2	120. LP* B1	6.95
129. LP O2	122. LP* B1	8.61
130. LP O2	120. LP* B1	41.15
130. LP O2	122. LP* B1	52.54
		Total: 115.93
M8-TS1$_{up\text{-}si}$		
130. LP O2	647. BD* C4–C3	24.69
128. LP O2	119. LP* B1	6.56
128. LP O2	121. LP* B1	10.87
129. LP O2	119. LP* B1	8.49
129. LP O2	121. LP* B1	19.41
		Total: 70.02

[a]Only the stabilization energies (*E*(2)) related to charge transfer between O2 and B1 greater than 5.00 kcal mol^{-1} are listed in the table.

the charge transfer interactions from O2 to B1. Comparison of the total stabilization energies of the competing transition states for the *(S)*-catalyst verifies that **M1-TS1**$_{down\text{-}si}$ exhibits considerably higher stabilization energy (128 kcal/mol) than **M2-TS1**$_{down\text{-}re}$ (80 kcal/mol). Likewise, for the *(R)*-catalyst, total stabilization energy is much greater for **M5-TS1**$_{down\text{-}re}$ (116 kcal/mol) compared to **M8-TS1**$_{up\text{-}si}$ (70 kcal/mol). Thus, we propose that stronger Lewis acid-base type coordination between B1 of the catalyst and O2 of the aldehyde is the major contributor to the stabilization of the transition state in enantio-determining step.

In order to shed light on the structural features determining the enantioselectivity of the aldol reaction, the structure of homoboroproline (***S***)**-5** was modified by Batsanov *et al.*[46] The extention of the carbon chain between proline and boronic acid group in the catalyst produced the longer-chain amino-boronic acids (***R***)-**5 a** and (***S***)-**5 b** (Figure 12). It was expected

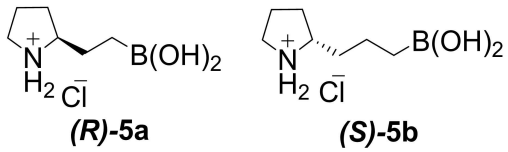

Figure 12. Homologous catalysts (***R***)-**5a** and (***S***)-**5b**

that this could remove the need for diol esterification. The aldol reaction under the same conditions of catalyst (***S***)-**5** was performed with the homologous catalysts (***R***)-**5 a** and (***S***)-**5 b**. Interestingly, very low yields with no asymmetric induction was observed. The authors ascribed this observation to the B–N chelation effect facilitated by longer and flexible carbon chain, enabling an intramolecular 5-membered B–N coordination and thus suppressing the aldol reaction presumably by disfavoring the enamine formation.[46] These observations also confirm our asymmetric induction model in which Lewis acid-base type interaction between boron and the aldehyde oxygen is required at the transition state. In the case of homologous catalysts (***R***)-**5 a** and (***S***)-**5 b**, even if some amount of enamine is formed, asymmetric induction will be lost because of the depletion of Lewis acidity of boron as a result of B–N chelation.

Conclusions

Herein, we report a comprehensive computational study to provide an insight into the factors governing the enantioselectivity. These calculations predict the most plausible pathway for the homoboroproline catalyzed aldol reaction. The addition of homoboroproline to the *re* or *si* face of aldehyde is identified as the enantio-determining step. The key factors influencing the selectivity of the aldol reaction are the boron-oxygen and carbon-carbon bond distances (Figure 13). The B1-O2 distance is decreased with a corresponding increase in the C3 and C4 distance.

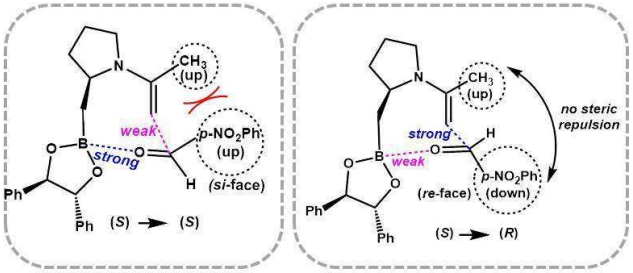

Figure 13. Key interactions responsible for the stereoselectivity of the homoboroproline catalyzed aldol reaction

A likely explanation for the stability of **M1-TS1**$_{down\text{-}si}$ (*S*→*S*) over **M2-TS1**$_{down\text{-}re}$ (*S*→*R*) is the strong interaction between the overlapping π-electron systems on the oxygen and boron in **M1-TS1**$_{down\text{-}si}$. We propose that the steric repulsion between the alkyl group of the enamine and phenyl group of the aldehyde provokes the charge transfer interaction between boron and the aldehyde oxygen which is validated by the second order perturbation theory analysis of the Fock matrix in the NBO. Thus, B–O coordination plays a key role in asymmetric induction of homoboroproline catalyzed aldol reaction.

In conclusion, theoretical results are in full accord with the experimental observations. These calculations provide significant insight into the understanding of asymmetric aldol reactions, in particular, the selectivity resulted from hydrobenzoin boronate ester catalyst.

Materials and methods

The conformation analysis of (***S***)-**10** has been carried out by Spartan 14 program package.[47] All the other computations presented in this work have been performed employing Gaussian 09, Revision B.01.[48] Geometry optimization and frequency calculations have been performed at the M06-2X[49,50] /6-31G(d,p) level of theory with a PCM[51] solvation model in acetone. The M06-2X functional has been chosen because of its good performance in predicting the activation energies and transition state geometries of various reactions.[49,52,53] Specifically, M06-2X functional has successfully reproduced the stereoselectivity in several asymmetric reactions involving boronate ester derivatives.[54,55,56] Harmonic vibrational frequencies have been calculated for all optimized structures to obtain thermal corrections at 298 K and to verify the nature of the stationary points in potential energy surfaces. Transition state structures have been characterized by only one imaginary frequency while minimum energy points were confirmed by no imaginary frequency. For key transition states, the intrinsic reaction coordinate (IRC)[57,58,59] paths have been traced to confirm each transition state leads to the expected reactants and products. Stabilization energies *E*(*2*) due to donor (*i*)–acceptor (*j*) interactions have been obtained from the second order perturbation theory analysis of the Fock matrix in NBO calculations.[43] The % ee values have been calculated from the

differences in Gibbs free energies of the TSs of selectivity-determining steps.[24]

Supporting Information Summary

Potential energy profiles of **M5**-**M10** including the discussion, cartesian coordinates and absolute energies of all calculated compounds can be found in the Supporting Information.

Acknowledgments

This work was supported by Marmara University, Scientific Research Projects Committee (BAPKO). Project Number: FEN–B-100615-0269. The numerical calculations reported in this paper were partially performed at TUBITAK ULAKBIM, High Performance and Grid Computing Center (TRUBA resources).

Conflict of Interest

The authors declare no conflict of interest.

Keywords: Aldol reaction · Boronate ester catalyst · Density functional calculations · Enantioselectivity · Natural Bond Orbitals

[1] C. A. Wurtz, *Bull. Soc. Chim. Fr.* **1872**, *17*, 436–442.
[2] R. Mahrwald, *Chem. Rev.* **1999**, *99*, 1095–1120.
[3] T. D. Machajewski, C.-H. Wong, *Angew. Chem., Int. Ed.* **2000**, *39*, 1352–1374.
[4] S. G. Nelson, *Tetrahedron: Asymmetry* **1998**, *9*, 357–389.
[5] H. Gröger, E. M. Vogl, M. Shibasaki, *Chem. Eur. J.* **1998**, *4*, 1137–1141.
[6] B. M. Trost, H. Ito, *J. Am. Chem. Soc.* **2000**, *122*, 12003–12004, and references therein.
[7] B. Alcaide, P. Almendros, *Angew. Chem. Int. Ed.* **2003**, *42*, 858–860, and references therein.
[8] I. Georgiou, A. Whiting, *Org. Biomol. Chem.* **2012**, *10*, 2422–2430, and references therein.
[9] G. J. Rowlands, *Tetrahedron* **2001**, *57*, 1865.
[10] Z. G. Hajos, D. R. Parrish, *J. Org. Chem.* **1974**, *39*, 1615–1621.
[11] B. List, *Tetrahedron* **2002**, *58*, 5573–5590.
[12] B. List, R. A. Lerner, C. F. III. Barbas, *J. Am. Chem. Soc.* **2000**, *122*, 2395–2396.
[13] W. Notz, B. List, *J. Am. Chem. Soc.* **2000**, *122*, 7386–7387.
[14] B. List, P. Pojarliev, C. Castello, *Org. Lett.* **2001**, *3*, 573–575.
[15] B. List, *Synlett* **2001**, *11*, 1675–1686.
[16] K. Sakthivel, W. Notz, T. Bui, C. F. III. Barbas, *J. Am. Chem. Soc.* **2001**, *123*, 5260–5267.
[17] P. I. Dalko, L. Moisan, *Angew. Chem. Int. Ed.* **2004**, *43*, 5138–5175 and references therein.
[18] H. Gröger, J. Wilken, *Angew. Chem. Int. Ed.* **2001**, *40*, 529–532.
[19] S. Bahmanyar, K. N. Houk, *J. Am. Chem. Soc.* **2001**, *123*, 11273–11283.
[20] K. N. Rankin, J. W. Gauld, R. J. Boyd, *J. Phys. Chem. A* **2002**, *106*, 5155–5159.
[21] M. Arnó, L. R. Domingo, *Theor. Chem. Acc.* **2002**, *108*, 232–239.
[22] S. Bahmanyar, K. N. Houk, H. J. Martin, B. List, *J. Am. Chem. Soc.* **2003**, *125*, 2475–2479 and references therein.
[23] F. R. Clemente, K. N. Houk, *Angew. Chem., Int. Ed.* **2004**, *43*, 5766–5768.
[24] Q. Peng, F. Duarte, R. S. Paton, *Chem. Soc. Rev.* **2016**, *45*, 6093–6107 and references therein.
[25] A. Armstrong, R. A. Boto, P. Dingwall, J. Contreras-Garcia, M. J. Harvey, N. J. Masona, S. H. Rzepa, *Chem. Sci.* **2014**, *5*, 2057–2071 and references therein.
[26] K. Arnold, A. S. Batsanov, B. Davies, C. Grosjean, T. Schütz, A. Whiting, K. Zawatzky, *Chem. Commun.* **2008**, 3879–3881 and references therein.
[27] R. L. Letsinger, S. H. Dandegaonker, W. J. Vullo, J. D. Morrison, *J. Am. Chem. Soc.* **1963**, *85*, 2223–2227.
[28] R. L. Letsinger, J. D. Morrison, *J. Am. Chem. Soc.* **1963**, *85*, 2227–2229.
[29] R. L. Letsinger, D. B. MacLean, *J. Am. Chem. Soc.* **1963**, *85*, 2230.
[30] R. L. Letsinger, S. H. Dandegaonker, *J. Am. Chem. Soc.* **1959**, *81*, 498–501.
[31] R. L. Giles, J. A. K. Howald, L. G. F. Patrick, M. R. Probert, G. E. Smith, A. Whiting, *J. Organomet. Chem.* **2003**, *680*, 257–262.
[32] S. W. Coghlan, R. L. Giles, J. A. K. Howard, M. R. Probert, G. E. Smith, A. Whiting, *J. Organomet. Chem.* **2005**, *690*, 4784–4793.
[33] K. Arnold, B. Davies, R. L. Giles, C. Grosjean, G. E. Smith, A. Whiting, *Adv. Synth. Catal.* **2006**, *348*, 813–820.
[34] A. J. Blatch, O. V. Chetina, J. A. K. Howard, L. G. F Patrick, C. A Smethurst, A. Whiting, *Org. Biomol. Chem.* **2006**, *4*, 3297–3302.
[35] A. S. Batsanov, D. Hérault, J. A. K. Howard, L. G. F. Patrick, M. R. Probert, A. Whiting, *Organometallics* **2007**, *26*, 2414–2419.
[36] A. S. Batsanov, C. Grosjean, T. Schütz, A. Whiting, *J. Org. Chem.* **2007**, *72*, 6276–6279.
[37] S. Arkhipenko, M. T. Sabatini, A. S. Batsanov, V. Karaluka, T. D. Sheppard, H. S. Rzepad, A. Whiting, *Chem. Sci.*, **2018**, *9*, 1058–1072.
[38] K. Aelvoet, A. S. Batsanov, A. J. Blatch, L. G. F. Patrick, C. A. Smethurst, A. Whiting, *Angew. Chem., Int. Ed.* **2008**, *47*, 768–770.
[39] K. Arnold, B. Davies, D. Hérault, A. Whiting, *Angew. Chem., Int. Ed.* **2008**, *47*, 2673–2676.
[40] I. Georgiou, A. Whiting, *Eur. J. Org. Chem.* **2012**, 4110–4113, and references therein.
[41] K. Sakata, H. Fujimoto, *J. Am. Chem. Soc.* **2008**, *130*, 12519–12526.
[42] J. H. Lai, Y. Liu, W. Wu, Y. Zhou, H. H. Maw, W. W. Bachovchin, K. L. Bhat, C. W. Bock, *J. Org. Chem.* **2006**, *71*, 512–519.
[43] A. E. Reed, L. A. Curtiss, F. Weinhold, *Chem. Rev.* **1988**, *88*, 899–926.
[44] K. Cakir, S. S. Erdem, V. E. Atalay, *Org. Biomol. Chem.*, **2016**, *14*, 9239.
[45] R. Maji, S. C. Mallojjala, S. E. Wheeler, *Chem. Soc. Rev.* **2018**, *47*, 1142–1158.
[46] A. S. Batsanov, I. Georgiou, P. R. Girling, L. Pommier, H. C. Shen, A. Whiting, *Asian J. Org. Chem.*, **2014**, *3*, 470–479.
[47] Spartan 14. Wavefunction Inc., **2014**, Irvine CA, USA. www.wavefun.com
[48] M. J. Frisch, G. W. Trucks, H. B. Schlegel *Gaussian 09, Revision B.01.* (Wallingford CT: Gaussian, Inc., 2009). (For the full citation see SI)
[49] Y. Zhao, D. G. Truhlar, *Theor Chem Acc.* **2008**, *120*, 215–241.
[50] Y. Zhao, D. G. Truhlar, *Acc Chem Res.* **2008**, *4*, 157–167.
[51] S. Miertus, E. Scrocco, J. Tomasi, *Chem. Phys.* **1981**, *55*, 117–129.
[52] S. E. Gunal, G. S. Gurses, S. S. Erdem, I. Dogan, *Tetrahedron.* **2016**, *72*, 2122–2131.
[53] A. A. Kaya, E. Salamci, A. Menzek, S. S. Erdem, E. Şahin, K. Ecer, *Tetrahedron.* **2017**, *73*, 5381–5388.
[54] M. N. Grayson, J. M. Goodman, *J. Am. Chem. Soc.* **2013**, *135*, 6142–6148.
[55] M. N. Grayson, J. M. Goodman, *J. Org. Chem.* **2013**, *78*, 8796–8801.
[56] B. Lin, P. Yu, C. Q. He, K. N. Houk, *Bioorg. Med. Chem.* **2016**, *24*, 4787–4790.
[57] C. Gonzalez, H. B. Schlegel, *J Chem Phys.* **1989**, *90*, 2154–2161.
[58] C. Gonzalez, H. B. Schlegel, *J Phys Chem.* **1990**, *94*, 5523–5527.
[59] K. Fukui, *Acc. Chem. Res.* **1981**, *14*, 363–368.

Submitted: May 14, 2019
Accepted: July 2, 2019